

Investigation of scalar–scalar-gradient filtered joint density function for large eddy simulation of turbulent combustion

Cite as: Phys. Fluids **33**, 035121 (2021); <https://doi.org/10.1063/5.0039025>

Submitted: 29 November 2020 . Accepted: 25 January 2021 . Published Online: 05 March 2021

 Mengyuan Yuan, Hengbin Zhang, and  Chenning Tong

COLLECTIONS

Paper published as part of the special topic on [In Memory of Edward E. \(Ted\) O'Brien](#)



View Online



Export Citation



CrossMark

ARTICLES YOU MAY BE INTERESTED IN

[Probability density functions for fluctuations in turbulent two-phase flames](#)

Physics of Fluids **33**, 035119 (2021); <https://doi.org/10.1063/5.0038908>

[An analytic probability density function for partially premixed flames with detailed chemistry](#)

Physics of Fluids **33**, 035117 (2021); <https://doi.org/10.1063/5.0038888>

[Turbulence topology evolution in weakly turbulent premixed flames](#)

Physics of Fluids **33**, 035110 (2021); <https://doi.org/10.1063/5.0039330>

Physics of Fluids

SPECIAL TOPIC: Tribute to
Frank M. White on his 88th Anniversary

SUBMIT TODAY!



Investigation of scalar–scalar-gradient filtered joint density function for large eddy simulation of turbulent combustion

Cite as: Phys. Fluids **33**, 035121 (2021); doi: [10.1063/5.0039025](https://doi.org/10.1063/5.0039025)
Submitted: 29 November 2020 · Accepted: 25 January 2021 ·
Published Online: 5 March 2021



View Online



Export Citation



CrossMark

Mengyuan Yuan,  Hengbin Zhang, and Chenning Tong^{a)} 

AFFILIATIONS

Department of Mechanical Engineering, Clemson University, Clemson, South Carolina 29634, USA

Note: This paper is part of the special topic, In Memory of Edward E. (Ted) O'Brien.

^{a)} Author to whom correspondence should be addressed: ctong@clemson.edu

ABSTRACT

The scalar–scalar-gradient filtered joint density function (FJDF) and its transport equation for large eddy simulation of turbulent combustion are studied experimentally. Measurements are performed in the fully developed region of an axisymmetric turbulent jet (with jet Reynolds number $U_j D_j / \nu = 40\,000$) using an array consisting of three X-wires and three resistance-wire temperature probes. Filtering in the cross-stream and streamwise directions is realized by using the array and by invoking Taylor's hypothesis, respectively. The FJDF and the terms in the transport equation are analyzed using their means conditional on the filtered scalar and the subgrid-scale (SGS) scalar variance. The FJDF is unimodal when the SGS scalar variance is small compared to its mean value. The scalar gradient depends weakly on the SGS scalar. For large SGS variance, the FJDF is bimodal and the gradient depends strongly on the SGS scalar; therefore, the often-invoked independence assumption is not valid. The SGS scalar under such a condition contains a diffusion layer structure and the SGS mixing is similar to the early stages of binary mixing. The isoscalar surface in the diffusion layer has a lower surface-to-volume ratio than that in a well-mixed scalar. The conditionally filtered diffusion of the scalar gradient has an S-shaped dependence on the scalar gradient, which is expected to be qualitatively different from that of a reactive scalar under fast chemistry conditions. However, because modeling is performed at a higher level and because the scalar–scalar-gradient FJDF contains the information about the scalar dissipation and the surface-to-volume ratio, the FJDF approach is expected to be more accurate than scalar filtered density function approaches and has the potential to model turbulent combustion over a wide range of Damköhler numbers.

Published under license by AIP Publishing. <https://doi.org/10.1063/5.0039025>

I. INTRODUCTION

Large eddy simulation (LES) is gaining increasing importance as an approach for computing turbulent reactive flows. The scalar filtered density function (FDF) method^{1–3} has been shown to be a highly effective method to account for the effects of subgrid-scale (SGS) mixing. The method solves the FDF transport equation in which the effects of reactions on the evolution of the FDF are in closed form. However, it has the limitation that it contains no information about the small-scale spatial structure. In addition, the effects of reactions on mixing (scalar diffusion) must be modeled; therefore, it is difficult to apply this approach to a wide range of Damköhler numbers without assumptions about the flame structure.

A higher-level approach solves the scalar–scalar-gradient filtered joint density function (FJDF) transport equation, in which the effects of reactions on the scalar gradient distribution are also in closed

form.^{4,5} The scalar–scalar-gradient FJDF contains the information about the scalar and its dissipation rate, which play a central role in the laminar flamelet,⁶ the quasi-equilibrium distributed reaction zones,⁷ and the conditional moment⁸ approaches for nonpremixed combustion. It also contains the isoscalar surface-to-volume ratio that is often used in modeling premixed combustion.⁴ Models for the evolution of the scalar–scalar-gradient joint probability density function (JPDF) have previously been developed^{9,10} and can, in principle, be adapted to the FJDF approach. To develop improved models used in the scalar–scalar-gradient FJDF approach, an understanding of the physics of the SGS scalar and the scalar-gradient fields is essential. In the present work, we investigate the scalar–scalar-gradient FJDF of a conserved scalar and its transport equation. In nonpremixed combustion, reactive scalars are strongly dependent on the mixture fraction, which is a conserved scalar. Therefore, the mixture fraction plays an

important role in understanding and modeling nonpremixed flames. An understanding of the FJDF of the mixture fraction and its gradient is a first step toward understanding that of reactive scalars.

The FJDF is defined as^{1,4}

$$\begin{aligned}
 f_{\phi\psi}(\hat{\phi}, \hat{\psi}; \mathbf{x}, t) &= \int \delta[\phi(\mathbf{x}', t) - \hat{\phi}] \prod_{i=1}^3 \delta[\psi_i(\mathbf{x}', t) - \hat{\psi}_i] G(\mathbf{x}' - \mathbf{x}) d\mathbf{x}' \\
 &= \langle \delta(\phi - \hat{\phi}) \prod_{i=1}^3 \delta(\psi_i - \hat{\psi}_i) \rangle_L,
 \end{aligned} \tag{1}$$

where $\hat{\phi}$ and $\hat{\psi}$ are the sample-space variables for the scalar ϕ and its gradient $\psi = \nabla\phi$, and δ and G are the Dirac delta function and the filter function, respectively. The integration is over all physical space. A filtered variable is denoted as $\langle \cdot \rangle_L$. The symbol $\langle \cdot \rangle$ is used for ensemble averages. The transport equation of the FJDF can be obtained using standard techniques,¹¹

$$\begin{aligned}
 \frac{\partial f_{\phi\psi}}{\partial t} + \frac{\partial}{\partial x_j} \left\{ \langle u_j | \hat{\phi}, \hat{\psi} \rangle_L f_{\phi\psi} \right\} &= - \frac{\partial}{\partial \hat{\phi}} \left\{ \left\langle D \frac{\partial^2 \phi}{\partial x_j \partial x_j} | \hat{\phi}, \hat{\psi} \right\rangle_L f_{\phi\psi} \right\} \\
 &\quad - \frac{\partial}{\partial \hat{\psi}_i} \left\{ \left\langle D \frac{\partial^2 \psi_i}{\partial x_j \partial x_j} | \hat{\phi}, \hat{\psi} \right\rangle_L f_{\phi\psi} \right\} \\
 &\quad + \frac{\partial}{\partial \hat{\psi}_i} \left\{ \left\langle \frac{\partial u_i}{\partial x_j} \psi_j | \hat{\phi}, \hat{\psi} \right\rangle_L f_{\phi\psi} \right\},
 \end{aligned} \tag{2}$$

where D is the molecular diffusivity and $\langle \cdot | \hat{\phi}, \hat{\psi} \rangle_L$ denotes a conditionally filtered variable conditional on the scalar and its gradient. The left-hand side is the time rate of change of the FJDF and advection of FJDF in physical space by the fluid velocity \mathbf{u} . The first term on the right-hand side represents transport in scalar space by the scalar diffusion, and the second and third terms represent transport in scalar-gradient space by the scalar-gradient diffusion and the scalar-gradient production. The alternatives to the two conditionally filtered diffusion terms are the scalar dissipation $\chi = D\psi_i\psi_i$, which is in closed form, the conditionally filtered scalar gradient dissipation $\langle D \frac{\partial \psi_i}{\partial x_j} \frac{\partial \psi_i}{\partial x_j} | \hat{\phi}, \hat{\psi} \rangle_L$, and the mixed scalar–scalar-gradient dissipation $\hat{\psi}_j \langle D \frac{\partial \psi_i}{\partial x_j} | \hat{\phi}, \hat{\psi} \rangle_L$.

The gradient of a conserved scalar in turbulent flows is generally considered to be a small-scale variable and is highly intermittent. According to Kolmogorov’s hypotheses, it is statistically independent of scalar fluctuations in high-Reynolds number, (quasi-) equilibrium flows. However, the scalar dissipation has been observed to depend on scalar fluctuations although their correlation coefficient is generally low in flows without large-scale intermittency.¹² In developing scalar fields or in highly intermittent regions of fully developed flows, the dependence can be significant. In the early stages of initially binary mixing, the scalar dissipation is strongly dependent on the scalar.¹³ The scalar gradient obtained in Monte Carlo simulations of binary mixing is also found to be dependent on the scalar.¹⁰ Significant correlations have also been observed in the developing region of a turbulent jet and near the wall of a turbulent boundary layer.¹⁴ Because of the role played by the scalar gradient in combustion modeling, the correlation is important and requires further investigations.

In the present work, we study the characteristics of the FJDF and some of the SGS terms in its transport equation. Unlike PDFs, an FJDF is not a statistic, but a random variable, and, therefore, must be characterized statistically. For a filter size smaller than the integral length scales, the (unconditioned) mean FJDF approximately equals the JPDF. Important characteristics of the FJDF can be revealed by its conditional means. Previous investigations of conditional scalar FDF and scalar–scalar-dissipation FJDF have shown that the SGS scalar at a given location in a flow is on average in equilibrium and in nonequilibrium for small and large instantaneous SGS variance, respectively.^{15–17} Here, for convenience, we refer to both the cases of the SGS production equal to and smaller than the dissipation as quasi-equilibrium because the corresponding SGS fields have very similar characteristics. For an equilibrium SGS scalar, the FDF is on average close to Gaussian and the scalar dissipation has only a moderate dependence on the SGS scalar. However, for a nonequilibrium SGS scalar at large SGS scalar variance, the FDF is bimodal and the scalar dissipation depends strongly on the SGS scalar. The SGS scalar is also characterized by the presence of a diffusion-layer structure (ramp-cliffs) previously observed.^{12,18} These characteristics are similar to the early stages of initially binary mixing.¹³ Because the SGS scalar in the equilibrium and nonequilibrium regimes is dominated by different structures and dynamics, the FJDF could potentially be modeled more accurately than the unconditioned FDF (or PDF), leading to improved LES statistics. In this work, we use velocity and passive temperature data obtained experimentally in the fully developed region of an axisymmetric turbulent jet to analyze the scalar–scalar-gradient FJDF and its transport equation.

II. FACILITIES AND APPARATUS

The jet facility was housed in a large, air conditioned room. The jet was produced with an assembly of a nozzle and a plenum chamber (Fig. 1), which contains a section of flow-straightening honeycomb and three stages of damping screens. The jet assembly was mounted vertically on a 5 × 5 ft² grill portion of the floor to allow the flow of entrainment air (Fig. 1). The flow downstream of the nozzle was surrounded by a circular screen (1/16” mesh size) of 6 ft in diameter to reduce the disturbances in the room. A collection hood at a downstream distance of 260 nozzle diameters (3.9 m) minimizes the effects of the ceiling on the jet. The hood was connected to an exhaust fan with the flow rate adjusted by a throttle. Jet air supply was heated with a pipe heater before entering the plenum chamber, producing an excess temperature (above the ambient) of 20 °C at the nozzle exit. The jet nozzle had a fifth-order polynomial profile with a large contraction ratio (≈100), producing a nearly top-hat velocity profile at the nozzle exit.

Measurements were performed for a jet exit velocity U_j of 40 m/s, which gives a jet Reynolds number Re_j of 40 000. The nozzle diameter D_j was 15 mm. The corresponding Taylor microscale Reynolds number $R_\lambda = \langle u_1^2 \rangle^{1/2} \lambda / \nu$ was approximately 230, where $\langle u_1^2 \rangle^{1/2}$ is the rms streamwise velocity fluctuation and λ is the Taylor microscale. Refer to Table I for other flow parameters. Data were collected at a downstream distance of $x/D_j = 80$ on the jet centerline, well into the self-similar (fully developed) region of the jet.

The mean axial velocity on the jet centerline U_c at this downstream location was 3.07 m/s, and the resulting U_j/U_c value was comparable to previous results.^{19–21} The excess mean temperature was

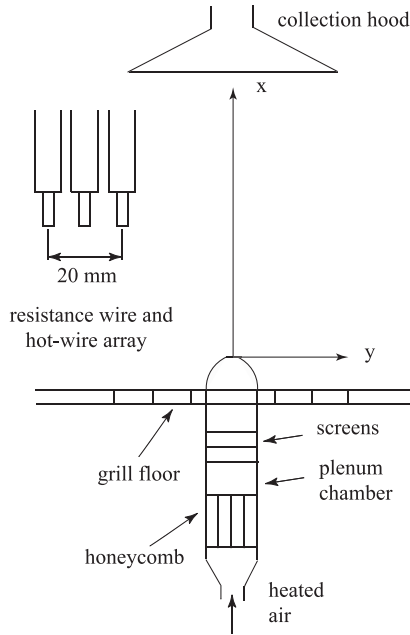


FIG. 1. A schematic of the experimental setup including a magnified view of the sensor array.

approximately 1.25 °C, and the normalized temperature was similar to those in previous studies.²² The Kolmogorov scale and the scalar dissipation length scale $\eta = (\nu^3/\epsilon)^{1/4}$ were 0.16 mm and 0.22 mm, respectively, where ϵ is the turbulent kinetic energy dissipation rate. Under these flow conditions The Kolmogorov frequency of the signals ($U_c/(2\pi\eta) = 2.5$ kHz) was fully resolved by the sensors. The non-buoyant (momentum dominated) region was determined to be $x/D_j \leq 196$ using a criterion based on a jet Froude number (the ratio of the square of the Reynolds number to the Grashof number) given by Chen and Rodi.²³ The effects of the initial jet-to-air density ratio (≈ 0.93) on the properties of the jet, such as the spreading rate and the rms fluctuations of velocity and temperature, were small.^{24,25} Thus, our measurement locations were well within the region in which the buoyancy effects were negligible and the temperature fluctuations were dynamically passive.

Measurements of the FJDF require spatial filtering of turbulent velocity and scalar fields. Due to the difficulties in obtaining three-dimensional data experimentally, two-dimensional (streamwise and radial directions) filtering is generally employed. In the present study, streamwise filtering was performed by invoking Taylor’s hypothesis and cross-stream filtering was realized with three hot-wire and resistance-wire sensors aligned in the cross-stream direction. The

TABLE I. Flow parameters on the jet centerline at $x/D_j = 80$. Here, $\langle u_1^2 \rangle^{1/2}$, $\langle u_2^2 \rangle^{1/2}$, R_λ , $\langle \epsilon \rangle$, η , $\langle \chi \rangle / \langle \phi^2 \rangle$, η_ϕ , and ℓ are the streamwise and cross-stream rms velocity fluctuations, the Taylor Reynolds number, the mean energy dissipation rate, the Kolmogorov length scale, the scalar dissipation (Corrsin) length scale, and the integral length scale, respectively.

$\langle U \rangle$	$\langle u_1^2 \rangle^{1/2}$	$\langle u_2^2 \rangle^{1/2}$	R_λ	$\langle \epsilon \rangle$	η	$\langle \chi \rangle / \langle \phi^2 \rangle$	η_ϕ	ℓ
3.07 m s ⁻¹	0.72 m s ⁻¹	0.61 m s ⁻¹	229	5.25 m ² s ⁻³	0.16 mm	5.52 s ⁻¹	0.22 mm	75 mm

TABLE II. SGS variances on the jet centerline at $x/D_j = 80$.

Δ/η (Δ/ℓ)	$\langle u_1''^2 \rangle$	$\langle u_2''^2 \rangle$	$\langle \phi''^2 \rangle / \langle \phi^2 \rangle$
63 (0.13)	0.107 m ² s ⁻²	0.089 m ² s ⁻²	0.189
125 (0.27)	0.174 m ² s ⁻²	0.140 m ² s ⁻²	0.317
250 (0.53)	0.261 m ² s ⁻²	0.205 m ² s ⁻²	0.462

X-wires are oriented such that the two measured velocity components are in the filter plane, while the resistance wires are placed near the X-wires. To minimize the error associated with invoking Taylor’s hypothesis, instantaneous convection velocity obtained by low-pass filtering the streamwise velocity component with a larger filter was used.

The array filter technique was proposed and studied by Tong *et al.*²⁶ for measurements in the atmospheric boundary layer and has been used by a number of authors to study the SGS stress²⁷ and conditional FDF.¹⁵ Two-dimensional filtering has been demonstrated to provide a very good approximation of three-dimensional filtering, with errors of approximately 5% for the rms of the resolvable-scale variables.²⁶ Previous studies of scalar FDF used box filters^{15,16,28} because a scalar FDF obtained with a box filter is easily interpreted. In this study, we also use box filters to maintain consistency between the SGS velocity and scalar fields. Our cross-stream array filter has a transfer function $\hat{G}_2(\kappa_2) = \frac{1}{3} + \frac{2}{3} \cos(\kappa_2 \Delta/2)$, which is somewhat narrower than a true box filter ($\hat{G}(\kappa_2) = \frac{\sin(\kappa_2 \Delta/2)}{\kappa_2 \Delta/2}$) in the wavenumber space, where Δ is the filter size. Our estimates using the spectral model for inertial-range isotropic turbulence show that the array filter overestimates the mean SGS energy and SGS scalar variance by approximately 13%. The mean SGS velocity variance $\langle u_1''^2 \rangle$ and $\langle u_2''^2 \rangle$ (double primes denote the SGS variables) is overestimated by 16% and 10%, respectively. These errors are not negligible but are not expected to have significant effects on the measured FJDF since much larger changes in the SGS variance ($\langle \phi''^2 \rangle_L$) are needed to alter the shape of the conditional FJDF (see Sec. III). Therefore, we expect that the box-array filter will produce FJDF statistics similar to those using a true two-dimensional box filter.

In the present study, three filter widths, 10, 20, and 40 mm, were used. These correspond to $\Delta/\ell = 0.13, 0.27, 0.53$, and $\Delta/\eta = 63, 125, 250$, respectively. Here, η ($= 0.16$ mm) is the Kolmogorov length scale. The scalar dissipation length scale η_ϕ is 0.22 mm. The integral length scale ℓ is estimated to be 75 mm using $\langle u_1^2 \rangle^{3/2} / \langle \epsilon \rangle$, where $\epsilon = 5\nu\{(\partial u_1/\partial x_1)^2 + (\partial u_2/\partial x_1)^2\}$. The percentages of the kinetic energy and the scalar variance contained in the SGS scales are given in Table II. The spectra of the streamwise velocity and resolvable-scale velocity are given in Ref. 17, which quantify the scales filtered.

Temperature fluctuations were measured with platinum resistance wires. Details of the devices are given in Ref. 28. Velocity

measurements were performed with three X-wire probes operated by TSI IFA 100 hot-wire anemometers with an overheat ratio of 1.8. The probes were calibrated using a modification of the method by Browne *et al.*^{17,29} Due to the high signal-to-noise ratio of the resistance-wire temperature device, a very low excess temperature (1.25 °C at the measurement location) can be used, rendering the temperature contamination of hot wires negligible. For the statistics considered, the differences between the corrected and uncorrected results are within 2%. Therefore, the uncorrected results are given.

The velocity and temperature signals were low-pass filtered at 5 kHz and amplified using Krohn-Hite 3364 filter/amplifiers. The signals were digitized at 10k samples/s using a 12-bit National Instrument A/D converter (PCI-6071E), which has a maximum sampling rate of 1.25×10^6 samples/s so that the interchannel delay is much shorter than the sample interval. In the present study, most of the statistics computed are conditional statistics with two to four conditioning variables. We achieve good statistical convergence by monitoring the results when the sample size is increased. We find that 2×10^8 data samples are sufficient.

III. RESULTS AND DISCUSSION

In this section, the results of the measured conditional FJDF and some of the terms in the FJDF transport equation are presented. Although the conditional scalar gradient is expected to be more intermittent as Δ/η (Δ/η_ϕ) increases, it is influenced more strongly by the SGS scalar variance and the results for the three filter sizes are qualitatively similar. Therefore, only results for $\Delta/\eta = 125$ are presented.

A. The conditional FJDF

The mean FJDF conditional on the SGS scalar variance and the resolvable-scale scalar $\langle f_{\phi\psi_1} | \langle \phi''^2 \rangle_L, \langle \phi \rangle_L \rangle$ is shown in Fig. 2. Note that for a specified value of the resolvable-scale scalar, the SGS scalar is equivalent to the total scalar. For convenience, we use ϕ'' and ψ_1 only and omit the sample-space variables $\hat{\phi}$ and $\hat{\psi}_1$ when plotting the FJDF. The FJDF is normalized by $\langle \phi''^2 \rangle_L^{1/2}$ and $(\chi_L/D)^{1/2}$ (χ_L defined as $\langle D(\partial\phi/\partial x_1)^2 \rangle_L$), with the latter being the rms scalar gradient in the filter domain. Figure 2 shows that for small SGS variance (generally $\langle \phi''^2 \rangle_L / \langle \phi''^2 \rangle \leq 1$), the conditional FJDF is unimodal. The FJDF is close to the product of the marginal conditional FDFs of ϕ and ψ_1 , indicating that the statistical dependence between the two variables is weak. The scalar–scalar-gradient JPDF measured at the same location, which is in the fully developed region of the turbulent jet, also has a similar shape¹⁴ although the correlation between ϕ and ψ_1 is slightly higher. Because a fully developed jet is in quasi-equilibrium, the similarity between the FJDF and the JPDF suggests that when the SGS variance is small, the SGS scalar is also in quasi-equilibrium and the scalar gradient has characteristics similar to those in an equilibrium flow.

For large SGS variance (generally $\langle \phi''^2 \rangle_L / \langle \phi''^2 \rangle > 3$), the FJDF [Fig. 2(b)] is bimodal with the two peaks near $\phi'' = \pm 1$ and $\psi_1 = 0$. The isocontours between $\phi'' = \pm 1$ have much larger values of $|\psi_1|$ compared to those of the product of the conditional marginal FDFs, indicating that the scalar gradient has much larger probabilities to take large values than those given by the marginal FDFs. Furthermore, the FJDF is strongly skewed to negative ψ_1 values. Therefore, the scalar gradient is strongly dependent on the SGS scalar for these ϕ'' values.

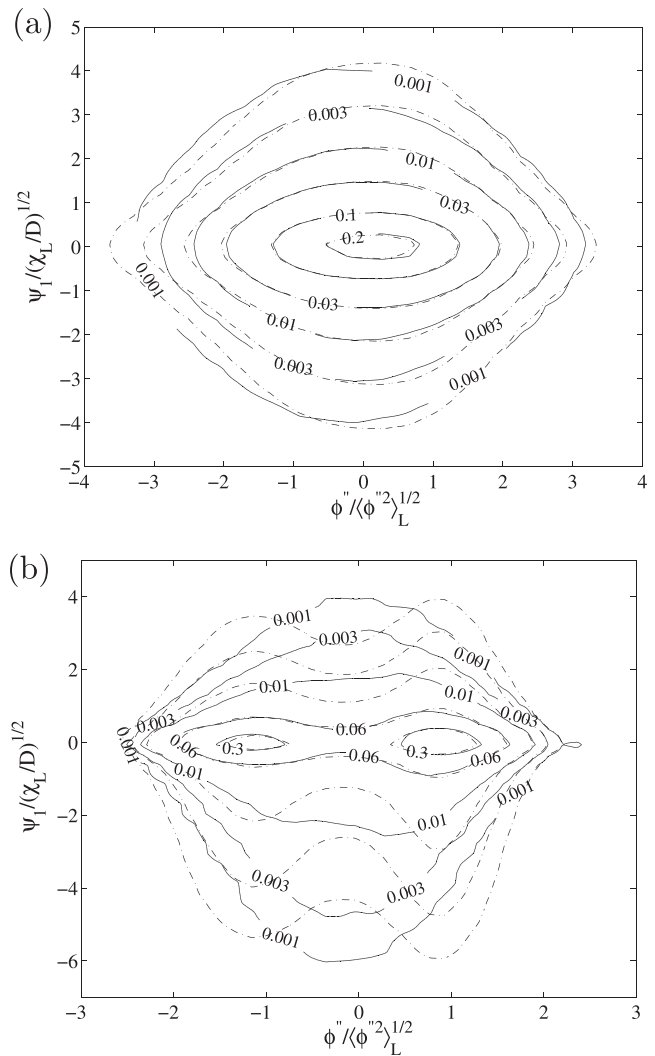


FIG. 2. Conditional mean of the FJDF on the jet centerline for $\langle \phi \rangle_L = \langle \phi \rangle$. (a) $\langle \phi''^2 \rangle_L / \langle \phi''^2 \rangle = 0.3$ and (b) 11.0. Solid and dashed isocontours are the conditional FJDF and the product of the marginal conditional FDFs, respectively.

For ϕ'' values beyond ± 1 , the dependence becomes somewhat weaker, suggesting that the SGS scalar in these regions is better mixed.

The FJDF results for large SGS variance are due to the presence of the diffusion layer structure in the SGS scalar. In such a structure, the gradient is largest near the center (cliff) where $\phi'' = 0$ and decreases toward the edges, resulting in a strong dependence of the gradient on the SGS scalar. The observed asymmetry of the FJDF in ψ_1 is due to the anisotropy of the scalar field: the scalar values are on average higher on the upstream side; therefore, cliffs with higher upstream scalar values ($\psi_1 < 0$) are more likely to occur.³⁰ Previous studies of conditionally filtered scalar dissipation and the scalar–scalar-dissipation FJDF^{16,28} are also consistent with the present results. Fox¹⁰ used one-dimensional layer-like lamella structures to model binary scalar mixing and obtained JPFDs qualitatively similar to the FJDF observed here. It would be interesting to compare the

FJDF with the JPDF from direct numerical simulations. The strong coupling between ϕ and ψ_1 shows that the independence assumption often invoked is not valid.

To further quantify the FJDF, we examine the conditional marginal FDF, $\langle f_{\psi_1|\phi} | \langle \phi \rangle_L, \langle \phi''^2 \rangle_L \rangle$ (Fig. 3). For small SGS variance, the conditional marginal FDF is only weakly dependent on ϕ'' (not shown), consistent with the results in Fig. 2(a). For large SGS variance, near $\phi'' = 1$ (and beyond), the conditional FDF has the classical stretched exponential shape of scalar gradient PDFs, again consistent with that of a well-mixed scalar. The slight skewness to the negative values is likely due to the residual anisotropy. For $\phi'' = 0$, which is near the center of the diffusion layer, the FDF decreases more slowly for $|\psi_1| < 6$. Beyond this range, the FDF appears to roll off at approximately the same rate as that for $\phi'' = \pm 1$. This suggests that the contributions of the cliffs to ψ_1 are largely limited to $|\psi_1| < 6$ (for higher SGS variance values, the limit is expected to be greater); therefore, the scalar gradient within cliffs is less intermittent than that outside. This is further evidenced by the kurtosis of the conditional marginal FDF (Fig. 4), which has two peaks near $\phi'' = \pm 1$ and a minimum near $\phi'' = 0$ (in the cliff). The peak kurtosis values are comparable to the scalar gradient kurtosis obtained in moderate Reynolds number flows.^{12,31}

The conditional FJDF also contains information about the density of isoscalar surfaces (e.g., the stoichiometric mixture fraction surface). The SGS isoscalar surface-to-volume ratio can be obtained as $\Sigma(\phi'') = f_\phi \langle |\psi_1| | \phi'' \rangle_L$. For small $\langle \phi''^2 \rangle_L$, $\Sigma(\phi'')$ has a shape close to Gaussian (Fig. 5). This is because the scalar FDF is close to Gaussian and the conditionally filtered scalar gradient magnitude has a moderate dependence on ϕ'' . For large $\langle \phi''^2 \rangle_L$, $\Sigma(\phi'')$ has a bimodal shape with a local minimum near $\phi'' = 0$, indicating that the SGS cliffs have a smaller surface density than the well-mixed SGS scalar. Therefore, in a reactive flow, when $\langle \phi''^2 \rangle_L$ is large, the reaction zones, which tend to occur in cliffs, are expected to be less wrinkled than those in a well-mixed region. The diffusion layer structure is similar to the mixture fraction structure in a laminar flamelet,³² and the lower surface density, which is equivalent to lower surface curvatures, further indicates that the structure is conducive to flamelets. By contrast, distributed

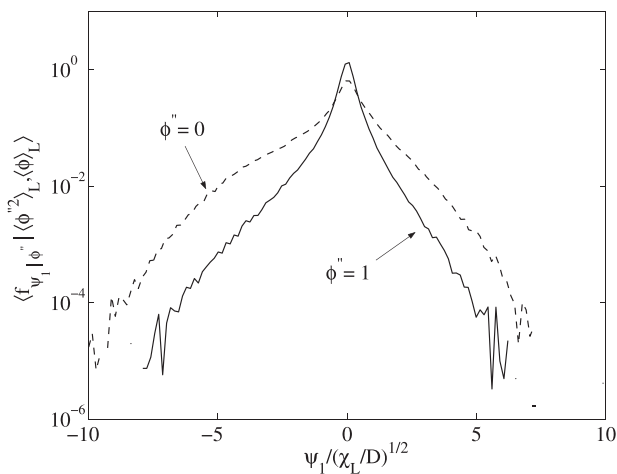


FIG. 3. Conditional mean of the FDF $\langle f_{\psi_1|\phi} | \langle \phi \rangle_L, \langle \phi''^2 \rangle_L \rangle$ for $\langle \phi''^2 \rangle_L / \langle \phi''^2 \rangle = 7.0$.

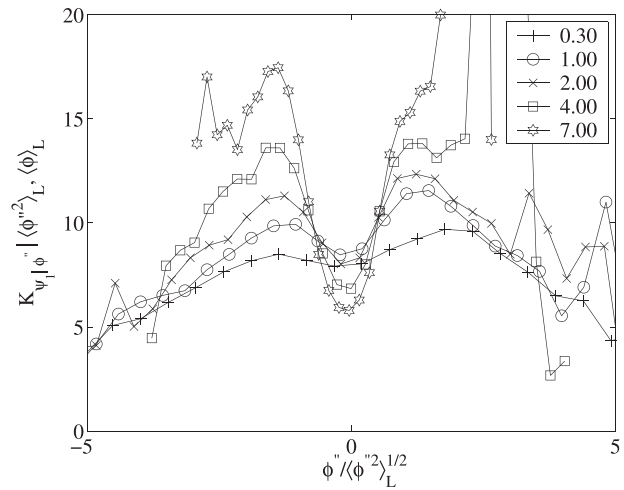


FIG. 4. Conditional kurtosis of the SGS scalar for the SGS variance values given in the legend.

reaction zones, which are more likely to occur in well-mixed mixture fraction fields, have higher curvatures.

B. The conditionally filtered scalar and scalar-gradient diffusion

In the present study, the scalar diffusion and scalar-gradient diffusion are also obtained using the streamwise derivatives. The conditionally filtered scalar diffusion $\langle \partial^2 \phi / \partial x_1^2 | \phi'', \psi_1 \rangle_L$ has a negative dependence on ϕ'' , similar to the conditionally filtered scalar diffusion conditional on ϕ alone ($\langle \partial^2 \phi / \partial x_1^2 | \phi'' \rangle_L$).¹⁶ The dependence becomes stronger with increasing ψ_1 (Fig. 6) because on average the diffusion is larger when mixing is stronger (large ψ_1). For $\psi_1 = 0$, the diffusion is small but non-zero, perhaps because the diffusion at local extrema has a zero gradient but non-zero diffusion. For large SGS variance values,

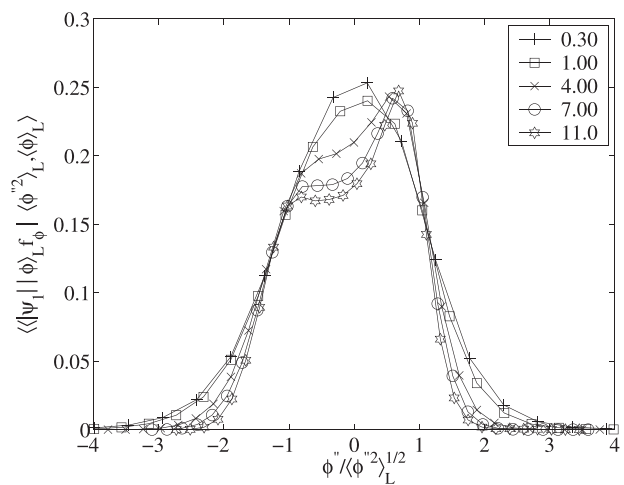


FIG. 5. Conditional isoscalar-surface density for the SGS variance values given in the legend.

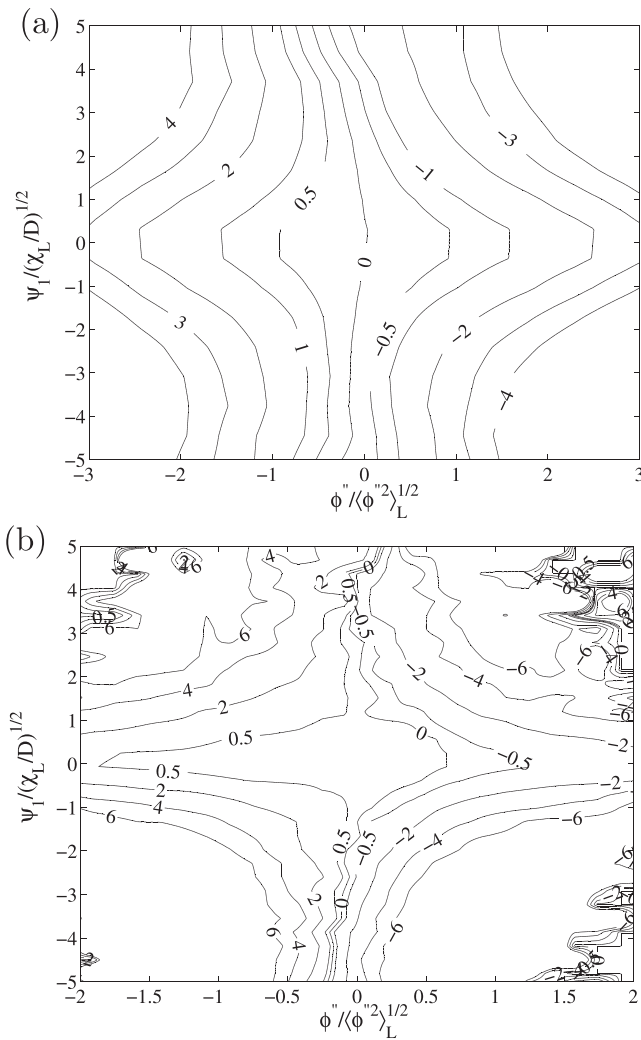


FIG. 6. Conditional scalar diffusion. The conditions are the same as in Figs. 2(a) and 2(b), respectively.

this qualitative feature is more pronounced, with the dependence weaker for small $|\psi_1|$ and stronger for large $|\psi_1|$. The dependence is especially strong for $\psi_1 < -3$. This is probably due to an ensemble of diffusion layers in the SGS scalar: in a diffusion layer, the diffusion is zero at the layer center and is largest near the edges where $\phi'' = \pm 0.7$, thus producing a strong dependence of the diffusion on ϕ'' for $|\phi''| < 0.7$. For $|\phi''| > 0.7$, the diffusion is not strongly affected by the diffusion layer and the dependence on ϕ'' and ψ_1 may become weaker, as suggested by the S-shaped diffusion conditioned on ϕ'' alone.¹⁶ The conditional diffusion term $\langle \partial^2 \phi / \partial x_1^2 | \phi, \psi_1 \rangle$ in the scalar-scalar-gradient JPFD transport equation measured at the same location in the jet (not shown) has a similar dependence on ϕ and ψ_1 . We note that although the scalar diffusion is not in closed form in the scalar-scalar-gradient FJFD approach, its alternative (the scalar dissipation term) is.

The conditionally filtered scalar-gradient diffusion shown in Fig. 7 has a negative, slightly S-shaped dependence on ψ_1 . Therefore,

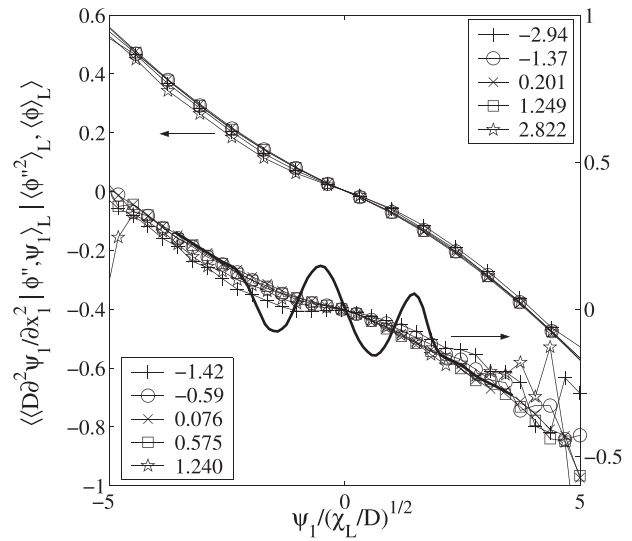


FIG. 7. Conditional scalar-gradient diffusion. The conditions are the same as in Fig. 2. The upper and lower curves are for small and large SGS variances, respectively. The thick solid line is a sketch of the diffusion of the gradient of a reacting scalar (e.g., Y_F) under fast chemistry conditions. The arrows point to the vertical coordinates for the curves.

molecular diffusion tends to pull the gradient toward the equilibrium point (usually the mean gradient), similar to its effects on the scalar. For large SGS variance, the S-shape appears to be more pronounced and the normalized magnitude of the gradient diffusion is smaller. This is due to the presence of diffusion layers. The scalar-gradient diffusion is close to zero away from a diffusion layer ($\psi_1 \approx 0$) and becomes negative near the edges of the layer (in a diffusion layer with a negative scalar jump), close to the layer center where ψ_1 has large negative values and $\partial^2 \psi_1 / \partial x_1^2$ becomes positive. Thus, the $\partial^2 \psi_1 / \partial x_1^2 - \psi_1$ curve has a dip at small negative ψ_1 values. A diffusion layer with a positive scalar jump will produce a diffusion curve that is anti-symmetric to that of a layer with a negative-jump, completing the S-shaped curve.

The dependence of the scalar-gradient diffusion on ϕ'' is generally weak for small SGS variance but becomes slightly stronger at large SGS variance. To further examine this, we compute the conditionally filtered gradient diffusion conditional on ϕ'' alone (not shown). For large $\langle \phi''^2 \rangle_L$, the gradient diffusion is positive near $\phi = 0''$ and becomes negative for large $|\phi''|$ values, qualitatively consistent with the diffusion layer structure.

In FDF methods, the effects of reactions on FDFs are in closed form. However, the effects on molecular diffusion must still be modeled. Generally, there are qualitative differences between the diffusion of a conserved scalar and that of a reacting scalar. For a conserved scalar, the conditionally filtered diffusion is linear or S-shaped, whereas for a reacting scalar (e.g., Y_F) under fast chemistry conditions, it has a bell shape centered at the stoichiometric mixture fraction (close to $Y_F = 0$).⁷ The conditionally filtered scalar-gradient diffusion of Y_F is also expected to have a different shape from that of a conserved scalar. A qualitative shape sketched in Fig. 7, which can be inferred from the laminar flamelet solution,³³ shows a rapid oscillation that is caused by

the reaction. Therefore, a mixing model for a conserved scalar gradient can potentially lead to unphysical prediction of mixing of reacting scalars. However, since in the $\phi - \psi$ FJDF approach, the effects of reactions on the scalar diffusion are modeled at a higher level compared to the scalar FDF approach, errors caused by a conserved-scalar mixing model are expected to be smaller.

The conditionally filtered production of scalar-gradient $-\langle \frac{\partial u_1}{\partial x_1} \psi_1 | \phi, \psi_1 \rangle_L$ has a positive dependence on ψ_1 (Fig. 8), while the dependence on ϕ'' is generally weak. The conditionally filtered velocity gradient $\langle \frac{\partial u_1}{\partial x_1} | \phi'', \psi_1 \rangle_L$ has an approximately symmetric linear dependence on ψ_1 (not shown). The increase in $-\frac{\partial u_1}{\partial x_1}$ with $|\psi_1|$ is expected as the production of ψ is mainly due to compressive strain rates acting on the scalar gradient. The approximate linear dependence is because on average the magnitudes of the dissipation-scale velocity and scalar fluctuations are generally proportional to each other (e.g., their rms fluctuations normalized by the rms integral-scale fluctuations scale as $Re_\ell^{1/4}$, where $Re_\ell^{1/4}$ is the turbulent Reynolds number). Therefore, the scalar gradient production has an asymmetric quadratic dependence on ψ_1 . Figure 8 shows that the dependence is stronger for larger SGS variance values, as diffusion layers tend to be associated with large strain rates.

C. The conditionally filtered scalar-gradient dissipation

The conditionally filtered scalar-gradient dissipation shown in Fig. 9 generally increases with both ϕ'' and ψ_1 . For small SGS variance, the isocontours are oval-shaped and there is a dependence on both ϕ'' and ψ_1 . The dependence on ϕ'' is similar to the dependence of the conditionally filtered scalar dissipation on the SGS scalar.¹⁶ For large SGS variance, the dependence on ϕ'' is weak for $|\psi_1| / (\langle \chi \rangle_L / D)^{1/2} < 1$ because a small gradient occurs mostly outside the diffusion layer where the gradient dissipation is also small. For large ψ_1 , the isocontours extend into regions of large ψ_1 and small ϕ'' values, consistent with small gradient dissipation values near the center of a diffusion

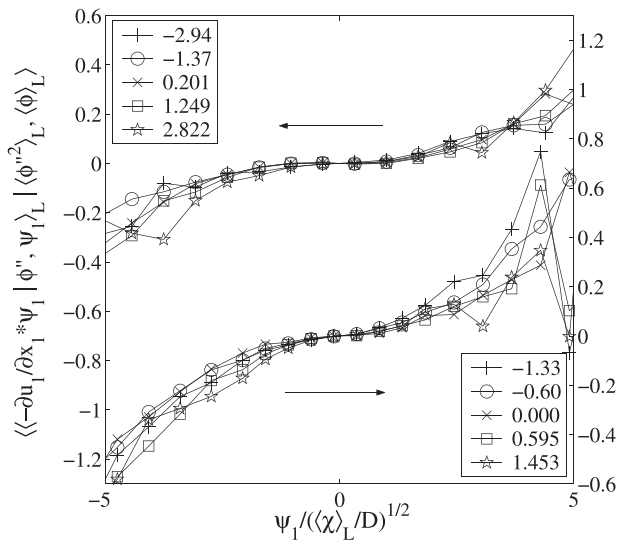


FIG. 8. Conditional scalar-gradient production. The upper and lower curves are for small and large SGS variances, respectively. The conditions are the same as in Fig. 2.

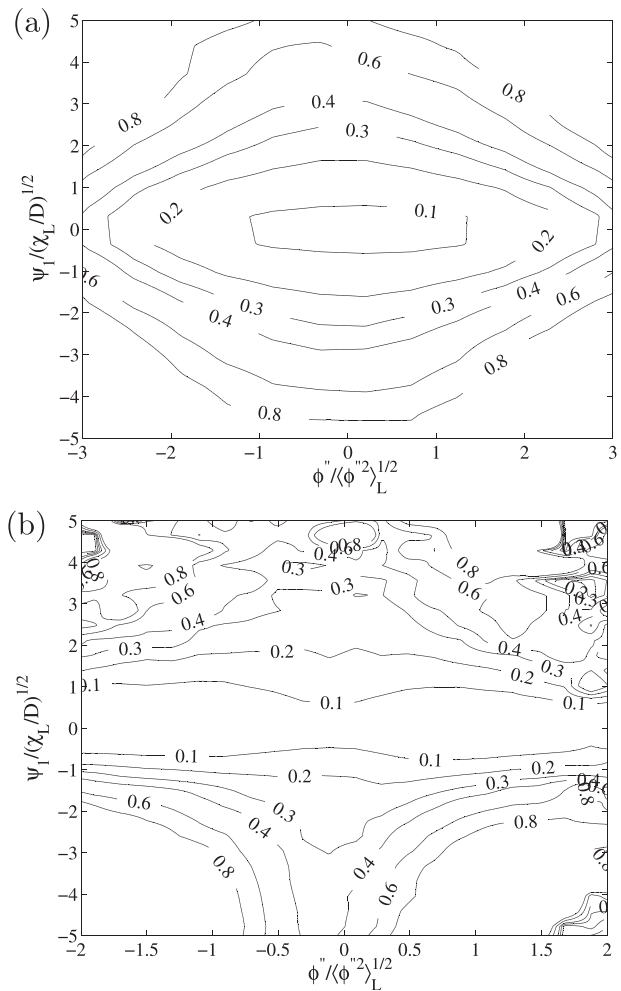


FIG. 9. Conditional scalar-gradient dissipation. The conditions are the same as in Figs. 2(a) and 2(b), respectively.

layer. Moving toward larger $|\phi''|$ with a fixed large ψ_1 value (e.g., ± 5), the dissipation increases sharply due to the large scalar-gradient dissipation near the edges of the diffusion layer. Again, mixing models need to predict the different characteristics of the scalar-gradient dissipation for small and large $\langle \phi''^2 \rangle_L$.

IV. CONCLUSIONS

The scalar-scalar-gradient FJDF and its transport equation were studied experimentally. Measurements were performed in the fully developed region (80 jet diameters downstream of the nozzle) of a heated turbulent air jet of Reynolds number 40 000. Velocity and temperature were obtained using an array consisting of three X-wire probes and three resistance-wire temperature probes. Filtering in the streamwise and cross-stream directions was performed by invoking Taylor’s hypothesis and using the array filter, respectively. The mean FJDF conditional on the filtered scalar and the SGS scalar variance, the conditionally filtered scalar diffusion, scalar-gradient diffusion, scalar-gradient production, and scalar-gradient dissipation were obtained.

In our analysis, qualitatively different results are obtained for small and large values of the SGS variance, $\langle \phi''^2 \rangle_L$. For small SGS scalar variance, the conditional FJDF is unimodal and the statistical dependence of the scalar gradient on the SGS scalar is weak. However, for large SGS variance, the FJDF is bimodal and the dependence of the gradient on ϕ'' is strong. Therefore, the independence assumption used in some modeling approaches is not valid. The results are consistent with the presence of diffusion layer structures that are similar to the mixture fraction structure in a laminar flamelet. The surface-to-volume ratio of such a structure is also smaller than that of an isoscalar surface in a well-mixed SGS scalar.

The conditionally filtered diffusion of ψ_1 has an S-shaped dependence on ψ_1 , which is more pronounced at large SGS variance due to the presence of the diffusion layer structure. The scalar-gradient diffusion of a reacting scalar under fast chemistry conditions is expected to be qualitatively different from that of a conserved scalar. The scalar-gradient production has a quadratic dependence on the scalar gradient, consistent with the expected linear dependence of the velocity gradient on the scalar gradient. The scalar gradient dissipation is also strongly affected by the diffusion layer structure. These characteristics are important for modeling the FJDF equation. In LES, the different structures and dynamics of the SGS scalar and scalar gradient under (instantaneous) equilibrium and nonequilibrium conditions (e.g., small and large SGS scalar variance) could potentially be modeled more accurately. In addition, in the scalar–scalar-gradient FJDF approach, modeling is performed at a higher level, and it is expected to be more accurate than scalar FDF approaches. Furthermore, because the FJDF contains the information about the scalar dissipation and the surface-to-volume ratio, the FJDF approach has strong potential for accurately modeling turbulent combustion over a wide range of Damköhler numbers.

ACKNOWLEDGMENTS

The support of the National Science Foundation under Grant Nos. CTS-0093532 (CAREER Award) and CBET-1333489 are gratefully acknowledged.

DATA AVAILABILITY

The data that support the findings of this study are available from the corresponding author upon reasonable request.

REFERENCES

- ¹P. J. Colucci, F. A. Jaber, P. Givi, and S. B. Pope, “Filtered density function for large eddy simulation of turbulent reacting flows,” *Phys. Fluids* **10**, 499–515 (1998).
- ²D. C. Haworth, “Progress in probability density function methods for turbulent reacting flows,” *Prog. Energy Combust. Sci.* **36**, 168–259 (2010).
- ³S. Liu and C. Tong, “Investigation of subgrid-scale mixing of reactive scalar perturbations from flamelets in turbulent partially premixed flames,” *Combust. Flame* **162**, 4149–4157 (2015).
- ⁴S. B. Pope, “Computations of turbulent combustion: Progress and challenges,” in *Proceedings of the 23rd Symposium (International) on Combustion* (1990), pp. 591–612.
- ⁵C. Dopazo, “Recent development in PDF methods,” in *Turbulent Reactive Flow*, edited by P. Libby and E. F. A. Williams (Academic Press, New York, 1994), pp. 375–474.
- ⁶N. Peters, “Laminar diffusion flamelet models in non-premixed turbulent combustion,” *Prog. Eng. Combust. Sci.* **10**, 319–339 (1984).
- ⁷R. W. Bilger, “The structure of turbulent nonpremixed flames,” in *Proceedings of the Twenty-Second Symposium (International) on Combustion* (1988), pp. 475–488.
- ⁸R. Bilger, “Conditional moment closure for turbulent reacting flow,” *Phys. Fluids A* **5**, 436–444 (1993).
- ⁹R. Meyers and E. E. O’Brien, “The joint PDF of a scalar and its gradient at a point in a turbulent flow,” *Combust. Sci. Technol.* **26**, 123 (1981).
- ¹⁰R. O. Fox, “Improved Fokker-Planck model for the joint scalar, scalar gradient PDF,” *Phys. Fluids* **6**, 334–348 (1994).
- ¹¹S. B. Pope, “PDF methods for turbulent reacting flows,” *Prog. Eng. Combust. Sci.* **11**, 119–192 (1985).
- ¹²C. Tong and Z. Warhaft, “On passive scalar derivative statistics in grid turbulence,” *Phys. Fluids* **6**, 2165–2176 (1994).
- ¹³V. Eswaran and S. B. Pope, “Direct numerical simulations of the turbulent mixing of a passive scalar,” *Phys. Fluids* **31**, 506–520 (1988).
- ¹⁴F. Anselmetti, H. Djeridi, and L. Fulachier, “Joint statistics of a passive scalar and its dissipation in turbulent flows,” *J. Fluid Mech.* **280**, 173–197 (1994).
- ¹⁵C. Tong, “Measurements of conserved scalar filtered density function in a turbulent jet,” *Phys. Fluids* **13**, 2923–2937 (2001).
- ¹⁶D. Wang and C. Tong, “Conditionally filtered scalar dissipation, scalar diffusion, and velocity in a turbulent jet,” *Phys. Fluids* **14**, 2170–2185 (2002).
- ¹⁷D. Wang, C. Tong, and S. B. Pope, “Experimental study of velocity filtered joint density function and its transport equation,” *Phys. Fluids* **16**, 3599–3613 (2004).
- ¹⁸K. A. Buch and W. J. A. Dahm, “Experimental study of the fine-scale structure of conserved scalar mixing in turbulent shear flows. Part 2. $sc \approx 1$,” *J. Fluid Mech.* **364**, 1–29 (1998).
- ¹⁹I. Wygnanski and H. Fiedler, “Some measurements in the self-preserving jet,” *J. Fluid Mech.* **38**, 577 (1969).
- ²⁰N. R. Panchapakesan and J. L. Lumley, “Turbulence measurements in axisymmetric jet of air and helium. Part 1. Air jet,” *J. Fluid Mech.* **246**, 197 (1993).
- ²¹H. J. Hussein, S. P. Capp, and W. K. George, “Velocity measurements in a high-Reynolds-number, momentum-conserving, axisymmetric, turbulent jet,” *J. Fluid Mech.* **258**, 31 (1994).
- ²²D. R. Dowling and P. E. Dimotakis, “Similarity of concentration field of gas-phase turbulent jets,” *J. Fluid Mech.* **218**, 109 (1990).
- ²³C. J. Chen and W. Rodi, *Vertical Turbulent Buoyant Jets* (Pergamon, 1980).
- ²⁴C. D. Richards and W. M. Pitts, “Global effects on the self-preservation behavior of turbulent free jets,” *J. Fluid Mech.* **254**, 417–435 (1993).
- ²⁵R. W. Schefer and R. W. Dibble, “Mixture fraction field in a turbulent non-reacting propane jet,” *AIAA J.* **39**, 64 (2001).
- ²⁶C. Tong, J. C. Wyngaard, S. Khanna, and J. G. Brasseur, “Resolvable- and subgrid-scale measurement in the atmospheric surface layer: Technique and issues,” *J. Atmos. Sci.* **55**, 3114–3126 (1998).
- ²⁷C. Tong, J. C. Wyngaard, and J. G. Brasseur, “Experimental study of subgrid-scale stress in the atmospheric surface layer,” *J. Atmos. Sci.* **56**, 2277–2292 (1999).
- ²⁸A. G. Rajagopalan and C. Tong, “Experimental investigation of scalar-scalar-dissipation filtered joint density function and its transport equation,” *Phys. Fluids* **15**, 227–244 (2003).
- ²⁹L. W. B. Browne, R. A. Antonia, and L. P. Chua, “Calibration of x-probes for turbulent flow measurements,” *Exp. Fluids* **7**, 201–208 (1988).
- ³⁰C. Tong and Z. Warhaft, “Scalar dispersion and mixing in a jet,” *J. Fluid Mech.* **292**, 1–38 (1995).
- ³¹Z. Warhaft, “Passive scalars in turbulent flows,” *Annu. Rev. Fluid Mech.* **32**, 203–240 (2000).
- ³²D. Wang, C. Tong, R. S. Barlow, and A. N. Karpetis, “Experimental study of scalar filtered mass density function in turbulent partially premixed flames,” *Proc. Combust. Inst.* **31**, 1533–1541 (2007).
- ³³N. Peters, *Turbulent Combustion* (Cambridge University Press, Cambridge, England, 2000).